Peer-reviewed version available at Metals 2019, 9, 904; doi:10.3390/met9080904

Article

Influence of heat treatment on the workability of modified 9Cr-2W steel with higher B content

Hyeong Min Heo[1]*, Jun Hwan Kim[2], Sung Ho Kim[2], Jong Ryoul Kim[3], Won Jin Moon[1]

[1]Gwangju center, Korea Basic Science Institute, 77 Yongbong-ro, Buk-gu, Gwangju, 61186, Republic of Korea; herhm87@naver.com; wjmoon@kbsi.re.kr

[2]Innovative Fuel Technology Development Division, KAERI, 989-111 Daedeok-daero, Yuseong-gu, Daejeon, 34057, Republic of Korea; junhkim@kaeri.re.kr; shkim7@kaeri.re.kr

[3]Department of Materials Engineering, Hanyang University, 55, Hanyangdaehak-ro, Sangnok-gu, Ansan-si, Republic of Korea; jina@hanyang.ac.kr

***Correspondence: herhm87@naver.com; Tel.:+82-62-712-4499**

Abstract: In this study, the effect of heat treatment was investigated to influence the occurrence of fracture during manufacturing process of Alloy B steel with boron contents as high as 130 ppm. As the content of boron increases, it affects the phase transformation temperature and texture. The development of {111}<uvw> components in the γ-fiber is affected depending on the austenite fraction after phase transformation. The Alloy B steel indicated that the increase in the boron content increased the α to γ phase transformation temperature such that sufficient transformation did not occur in the normalizing condition. The cracks occurred at the point of the transition from elastic to plastic deformation in the ND direction during the rolling process, thereby resulting in failure. Therefore, it is necessary to avoid the intermediate heat treatment condition in which γ-fiber does not fully develop, i.e., an imperfect normalization.

Keywords: Modified 9Cr-2W steel, Boron content, Phase transformation, Texture, Heat treatment

1. Introduction

Nuclear power generation plays a key role in the Korea energy with low costs of raw materials and excellent base load capacity, however its enlargement is limited due to problem of spent nuclear fuel after operation. To solve these problems, it is necessary to develop an innovative nuclear power plant which can contribute to sustainable development, environmental protection and preparation for rapidly increasing energy consumption [1,2].

Recently, research has carried out to develop sodium cooled fast reactor (SFR) because it has many advantages in terms of economic efficiency, stability, nuclear non-proliferation and reducing the emission of spent nuclear fuel. It is designed to operate at temperature much higher than those in light water reactors and to improve thermal efficiency [3–7]. Nuclear fuel cladding tube which transfers efficient the fission energy and confines nuclear fuel rod and fissile material is a main component. Hence, the development of fuel cladding tube is essential as it is the most important component directly related to the safety of nuclear reactor.

Ferritic-martensitic (FM) steels have been considered as fuel cladding and duct materials for a SFR owing to their high thermal conductivities, low expansion coefficients and superior irradiation swelling compared to austenitic steel [8–10]. However, the creep rupture strength of FM steels abruptly decreases during long term creep exposure at high temperature [11]. An advanced FM steel alloy was developed on the basis of Gr.92 steel. Minor alloying elements such as B, N, Nb, Ta, and C

were optimized to achieve better mechanical properties at a high temperature [10]. Subsequently, we tested 36 model alloys of ingots by adjusting the B and N contents in 9Cr-2W steel, and the two model alloys of ingots with the best creep characteristics were designed into cladding tubes [12]. Research on the material property and the manufacturing technology of these alloys will considerably contribute to extend their applicability of nuclear reactor parts requiring the high temperature and creep characteristic in the future.

The optimum heat treatment conditions and the amount of cold working were determined through previous studies on manufacturing process parameters such as cold rolling rate, normalizing and tempering heat treatment temperature and time [8]. However, when rolling an Alloy B steel plate with B contents as high as 130 ppm, fracturing only occurred when the plate was subjected to tempering heat treatment after normalization. In addition, similar phenomena occurred under the same conditions in the cold drawing process. The fracture during the manufacturing process caused the production yield of the Alloy B to be reduced, resulting in low productivity.

In this study, the cause of fracture during the manufacturing process of Alloy B steel with low production yield were investigated to introduce the manufacturing process which improves the formability. The rolled specimens of Alloy B and Gr.92 steels according to the intermediate heat treatment conditions were observed using optical microscope (OM), stereoscope and electron backscatter diffraction (EBSD). In addition, the rolled specimens were carried out compression test to evaluate the mechanical properties along the orientation.

2. Materials and Methods

2.1 Materials

The chemical compositions of the two different kinds of 9Cr-2W steel, designated Alloy B and Gr.92, are shown in Table 1. In order to evaluate the formability of Alloy B steel according to heat treatment condition, plate specimens were manufactured as follows. Ingots were prepared using a vacuum induction melting (VIM) process and were fabricated into a round bar undergoing a hot forging process. The round bar was drawn to a 100 mm outer diameter. It was normalized at 1050 °C for 6 minutes, followed by air cooling at 298K (hereinafter, referred to as AC). Tempering treatment of the normalized specimens was carried out at 800 °C for 6 minutes, followed by AC. Reference material, Gr.92 with 200 mm outer diameter, was purchased and tested. Gr. 92 was normalized 1040 °C for 5 hours, followed by AC. Tempering treatment of the normalized specimens was carried out at 760 °C for 8 hours, followed by AC. For the same initial heat treatment, the normalizing and tempering conditions of the Gr.92 steels were carried out under the same conditions as Alloy B steel. Both materials had an outer diameter of 100 mm, and their thickness was 5 mm thickness.

Table 1 Chemical composition of Alloy B and Gr.92 steel (wt. %)

	C	Si	Mn	Ni	Cr	Mo	W	V	Nb	Ta	N	B
Alloy B	**0.07**	**0.10**	**0.45**	**0.45**	**9.0**	**0.5**	**2.0**	**0.20**	**0.2**	**0.05**	**0.02**	**0.013**
Gr.92	**0.1**	**0.45**	**0.44**	**0.49**	**9.0**	**0.46**	**1.60**	**0.20**	**0.07**	**-**	**0.04**	**0.004**

The specimen was rolled from a 5 mm to a 3 mm thickness which is in accordance with a reduction ratio of 40%, and then subjected to a heat treatment conditions. The tempering treatment

of rolled specimens were only carried out at 800 °C for 6minutes, followed by AC. Other heat treatment condition were normalized at 1050 °C and 1150 °C for 6, 15 and 30 minutes, followed by AC, respectively and then tempered at 800 °C for 6minutes, followed by AC. A schematic diagram of the experimental procedure is shown in Figure 1.

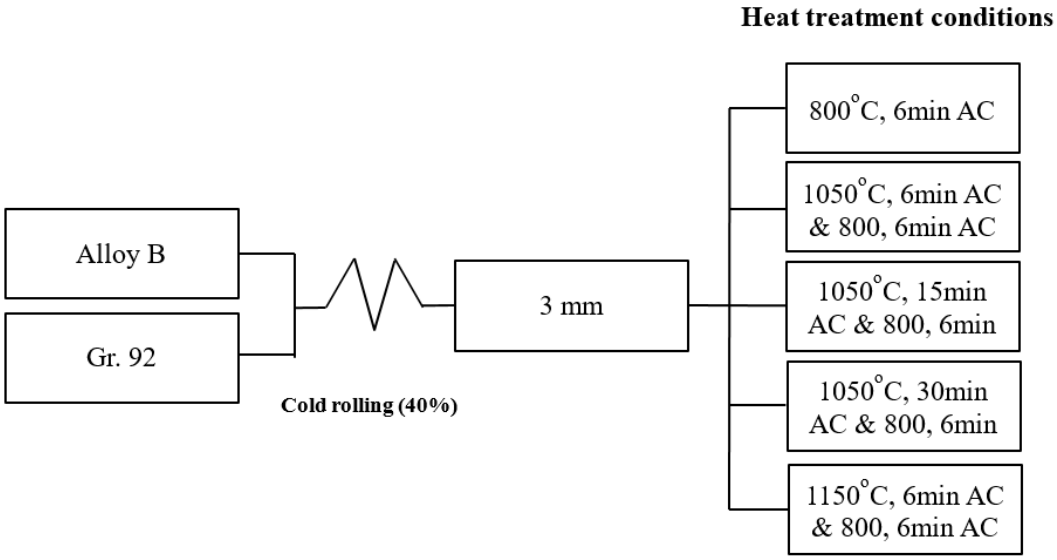

Figure 1 A schematic diagram of the experiment procedure.

2.2 Observation of microstructure

The microstructures of Alloy B and Gr.92 after the heat treatment conditions were investigated by OM, and EBSD after a metallographic sample preparation step. Specimens for the microstructural observations were grinded, polished (using diamond suspension of up to 0.25 ㎛) and etched (95 mL water + 3 mL nitric acid + 2 mL fluoric acid). The microstructures after the heat treatment conditions were investigated by EBSD after a metallographic sample preparation step. An additional one-hour polishing step with a 0.04 ㎛ colloidal silica suspension was then performed. Additionally, EBSD patterns were obtained using a Su5000 instrument equipped with a Hikari detector operated with EDAX-TSL OIM DATA collection software. Crystallographic textures that formed during various heat treatment processes were determined by the EBSD analysis. Orientation distribution functions (ODFs) $f(g)$ were calculated by the harmonic series expansion method based on Bunge (l = 22) from their incomplete pole figure {110}, {200}, and {211} [13,14]. Orientation g was expressed in the form of a triple Euler angle (φ_1, Φ, φ_2). All ODF calculations were conducted under the assumption of triclinic sample symmetry as given by the rolling direction (RD), transverse direction (TD), and normal direction (ND) of a plate such that $0^o \leq \{\varphi_1, \Phi, \varphi_2\} \leq 90^o$.

2.3 Compression test

Validity of the compression test as a general method of evaluating cold workability is investigated [15–17]. Compression test was performed at room temperature and strain rate of 1mm/min using an INSTRON-3367 to evaluate the mechanical properties and workability of the Alloy B and Gr.92 under the specific heat treatment conditions. The sampling of specimens and the compression test method are shown in Figure 2. The specimens were obtained from three directions, i.e., RD, TD and ND of rolled plate. These specimens were square of 2 mm x 2 mm x 2 mm and

finished to form smooth surface. Actual displacement and load were recorded continuously during the compression test. In addition, the occurrence of crack in the specimen was observed.

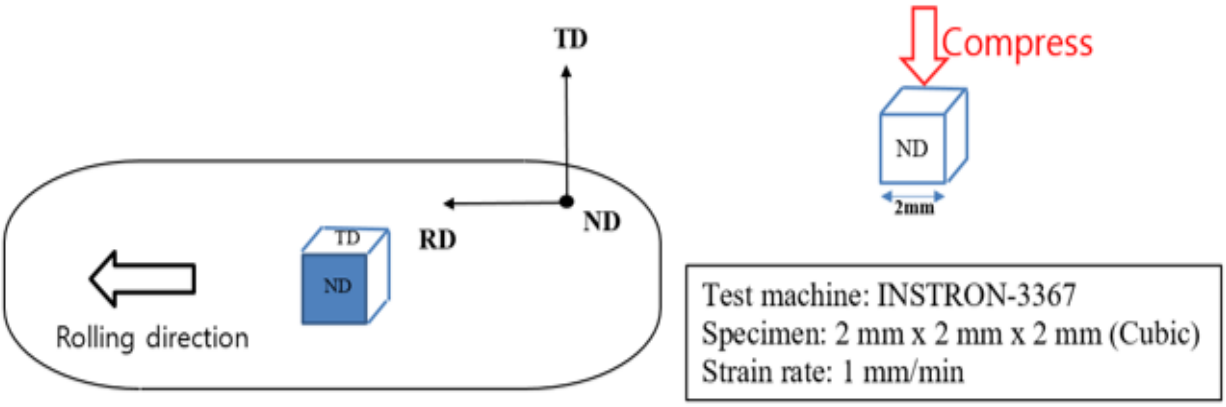

Figure 2 The sample and compression method.

3. **Result**

3.1 SEM and OM observation of the fracture surface of Alloy B and Gr.92 steel under different heat treatment conditions.

Typical fracture surface that occurred during the rolling process under the condition normalized and tempered plate of the Alloy B steel are shown in Figure 3. The Alloy B plate were characterized using SEM to evaluate the mode of fracture are shown in Figure 3 (b). The fracture surface denotes the presence of transgranular cleavage facets. The fractograph clearly revealed the brittle mode of fracture.

The OM images of Alloy B and Gr.92 steel based on the different heat treatment conditions are shown in the Figures 4 and 5, respectively. The rolling process formed an elongated grain boundary in the rolling direction of specimen. Elongated grain boundary appears in the tempered condition (800 °C, 6 minuates) of the Alloy B and Gr.92 steel without normalizing heat treatment. However, the heat treatment condition of 1050 °C, 6 minutes, and 800 °C, 6 minutes in the Alloy B steels resulted in the elongation of grain boundaries and deformation of the structure. Except for the aforementioned heat treatment conditions, the remainder represent tempered lath martensite structure.

Preprints (www.preprints.org) | NOT PEER-REVIEWED | Posted: 16 July 2019 doi:10.20944/preprints201907.0193.v1

Peer-reviewed version available at Metals 2019, 9, 904; doi:10.3390/met9080904

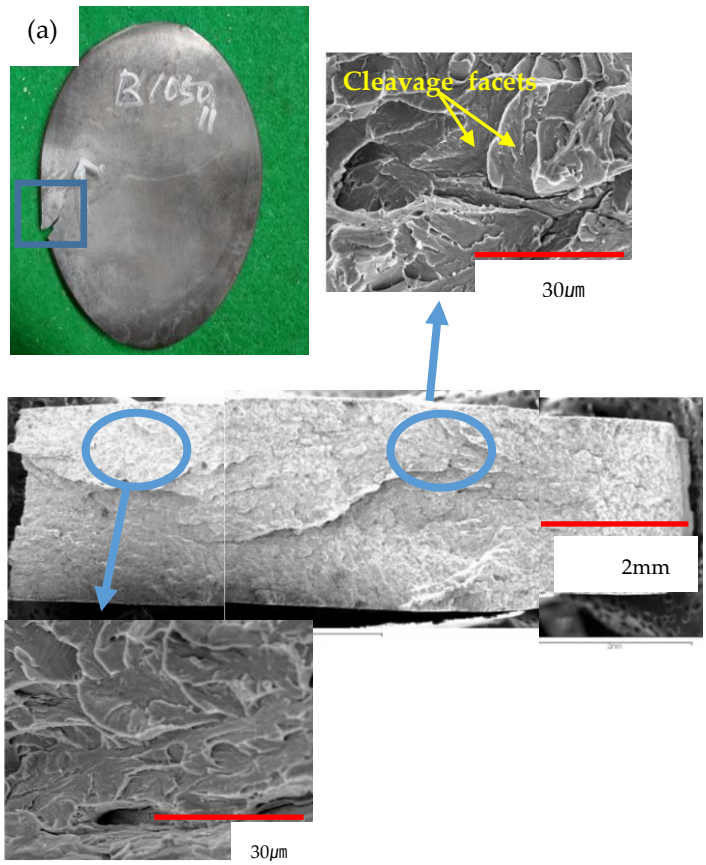

Figure 3 Fractograph and SEM images of Alloy B steel during rolling process under condition tempering after normalizing.

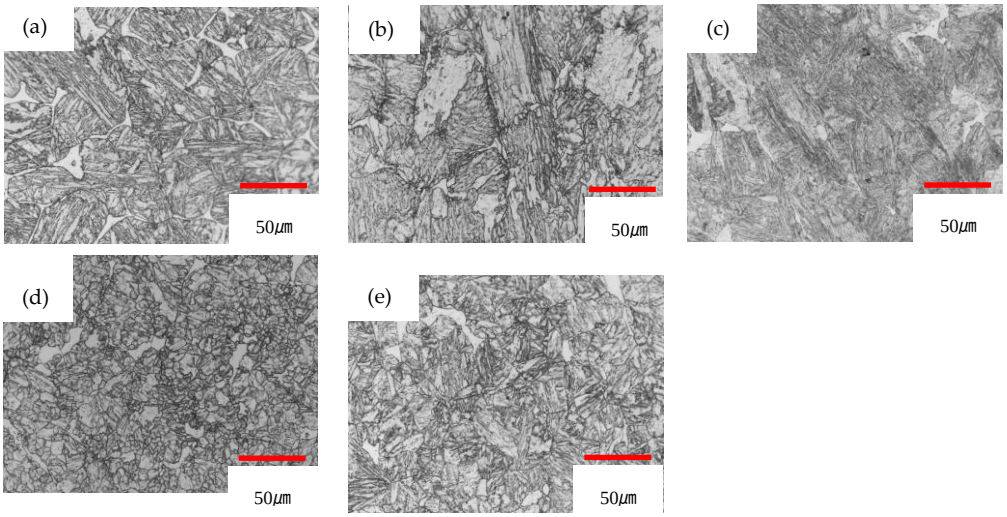

Figure 4 Optical micrographs of Alloy B steel with different intermediate heat treatment conditions: (a) As received (b) 800 °C, 6 minutes, (c) 1050 °C, 6 minutes, and 800 °C, 6 minutes, (d) 1050 °C, 30 minutes, and 800 °C, 6 minutes, and (e) 1150 °C, 6 minutes, and 800 °C, 6 minutes.

Preprints (www.preprints.org) | NOT PEER-REVIEWED | Posted: 16 July 2019 doi:10.20944/preprints201907.0193.v1

Peer-reviewed version available at Metals 2019, 9, 904; doi:10.3390/met9080904

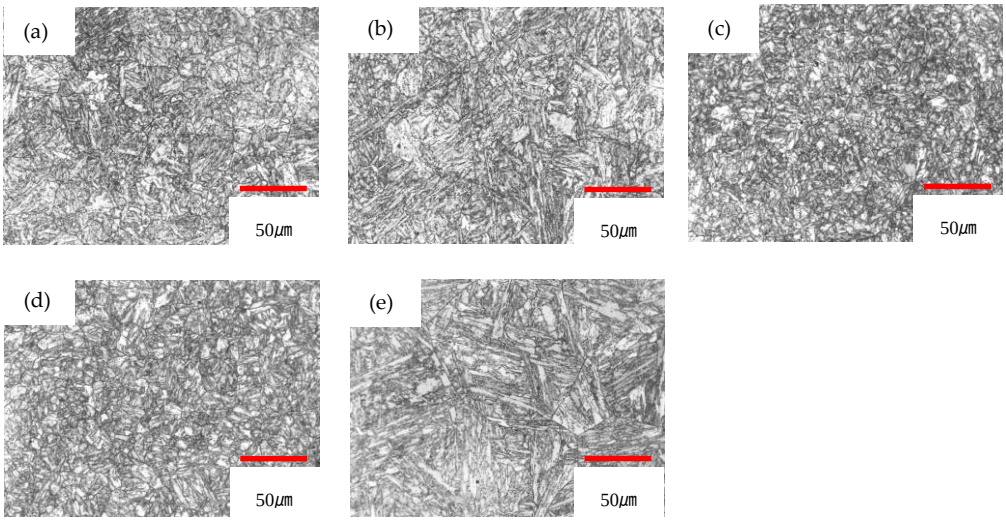

Figure 5 Optical micrographs of Gr.92 steel with different intermediate heat treatment conditions: (a) As received (b) 800 °C, 6 minutes, (c) 1050 °C, 6 minutes, and 800 °C, 6 minutes, (d) 1050 °C, 30 minutes, and 800 °C, 6 minutes, and (e) 1150 °C, 6 minutes, and 800 °C, 6 minutes.

3.2 Texture

The typical main texture components in cold-rolled low-carbon steels in the $\varphi 2 = 45^{o}$ section of the ODF are shown in Figure 6 [18]. The bcc metals and alloys tend to form α-fibers and γ-fibers. The α-fibers exhibited orientation and common <110> crystal axis parallel to the RD, i.e., the orientations {hkl}<110> which include the orientations {001}<110>, {112}<110>, and {111}<110> at (φ_1, Φ, φ_2) = (0^{o}, 0^{o}, 45^{o}), (0^{o}, 35^{o}, 45^{o}), and (0^{o}, 54.7^{o}, 45^{o}) in the Euler space. The γ-fibers consisted of orientations with the {111} crystal axis parallel to the ND i.e., the orientations {111}<uvw> which include the orientations {111}<110> and {111}<112> at (φ_1, Φ, φ_2) = (60^{o}, 54.7^{o}, 45^{o}) and (90^{o}, 54.7^{o}, 45^{o}) in the Euler space. Additionally, the Goss orientation {011}<100> is typically observed at (90^{o}, 90^{o}, 45^{o}) in the Euler space [18,19].

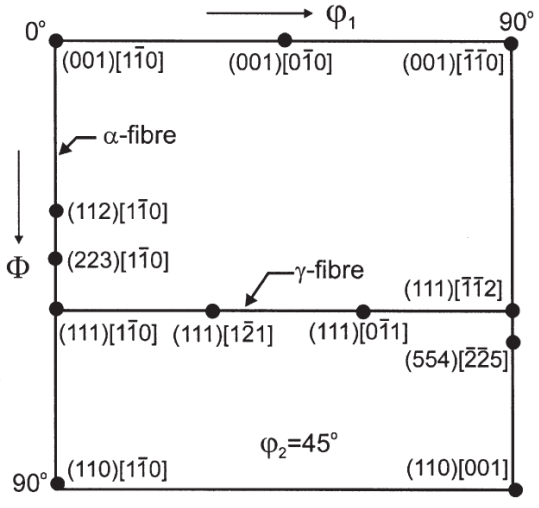

Figure 6 The main texture components typical in the cold-rolled low carbon steels in the $\varphi_2 = 45^{o}$ section of the orientation distribution function (ODF) [18].

The ODF outcomes for $\varphi_2 = 45^{o}$ section after different heat treatment conditions in the Alloy B and Gr.92 steels are shown in Figures 7 and 8 (a) – (e). The evolution outcomes of γ-fiber through the

intensity of the ODF based on the heat treatment used are shown in Figure 9. All the heat treatment condition of Alloy B and Gr.92 steel resulted in the development of α-fibers that exhibited orientation and a common <110> crystal axis parallel to the RD. In the Alloy B steel, as received and 1050 °C, 6 minutes, and 800 °C, 6 minutes conditions did not develop the γ-fiber components which is advantageous for formability. Except for the aforementioned heat treatment conditions, the γ-fiber components was developed. On the other hand, Gr.92 steel has developed γ-fiber components under all conditions. The reason why the γ-fiber components was uniformly developed in all heat treatment conditions after rolling because the γ-fiber components was developed in the initial condition.

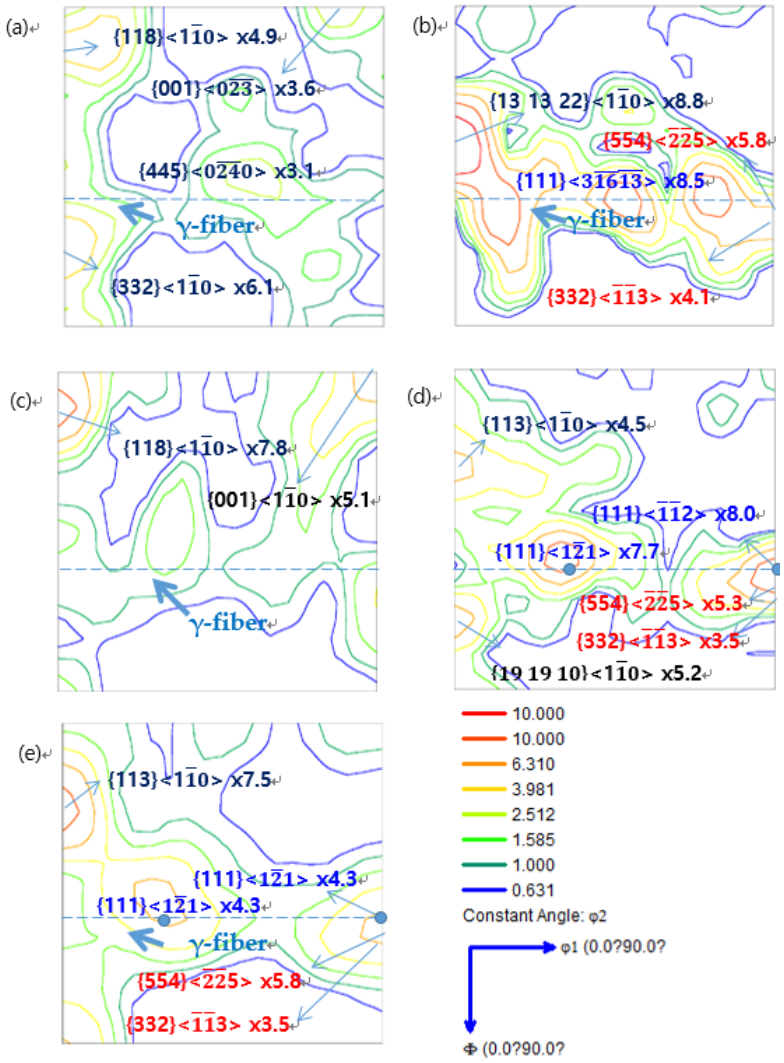

Figure 7 φ_2 = 45° section of ODF in the Alloy B steel: (a) as received, (b) 800 °C, 6 minutes, (c) 1050 °C, 6 minutes, and 800 °C , 6 minutes, (d) 1050 °C, 30 minutes, and 800 °C, 6 minutes, and (e) 1150 °C, 6 minutes, and 800 °C , 6 minutes.

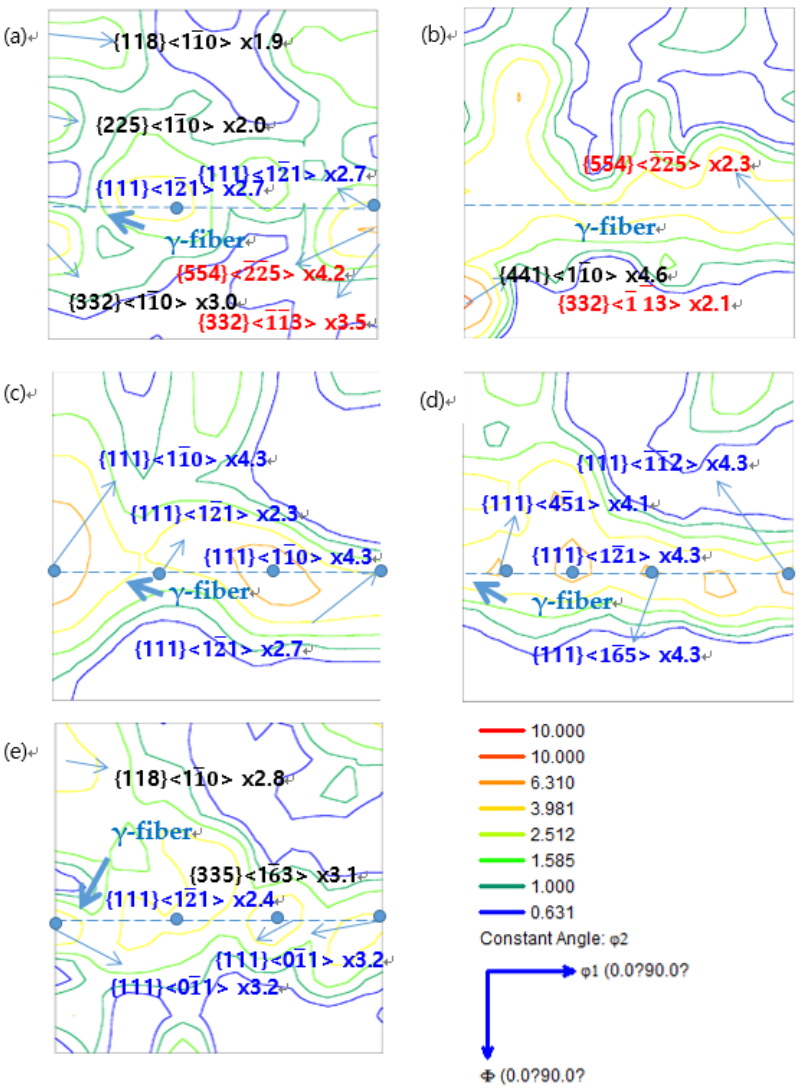

Figure 8 $\varphi_2 = 45°$ section of ODF in the Gr.92 steel: (a) as received, (b) 800 °C, 6 minutes, (c) 1050 °C, 6 minutes, and 800 °C, 6 minutes, (d) 1050 °C, 30 minutes, and 800 °C, 6 minutes, and (e) 1150 °C, 6 minutes, and 800 °C, 6 minutes.

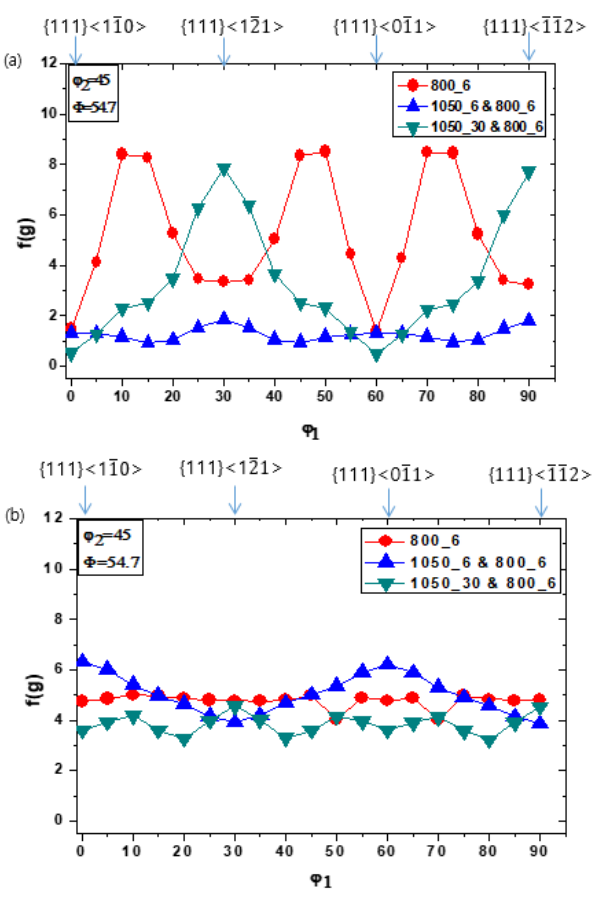

Figure 9 Evolution of the ODF intensity *f(g)* with different intermediate heat treatment conditions in the γ-fiber (Φ= 54.7° and φ_2 = 45°, constant): (a) Alloy B and (b) Gr.92.

3.3 Effect of Heat Treatment Conditions on Mechanical Properties

The results of the compression tests along the ND direction of the Alloy B and Gr.92 steel at 298K are shown in Figure 10. The same compression test results were shown for all conditions excluding the compression test in the ND direction of the 1050 °C, 6 minutes, and 800 °C, 6 minutes condition. With respect to the compression test in the ND direction of the Alloy B, hardening and strength rapidly increased in the elastic region. Therefore, fracture occurred during the transition from elastic to plastic region. The results of the compression test image in the ND direction are shown in Figure 11. In the Gr.92 condition, wherein the rolling was successful without fracture, cracks were absent in all directions. In the case of the Alloy B at 1050 °C, 6 minutes, and 800 °C, 6 minutes condition (wherein fracture was observed), there were cracks in the ND direction.

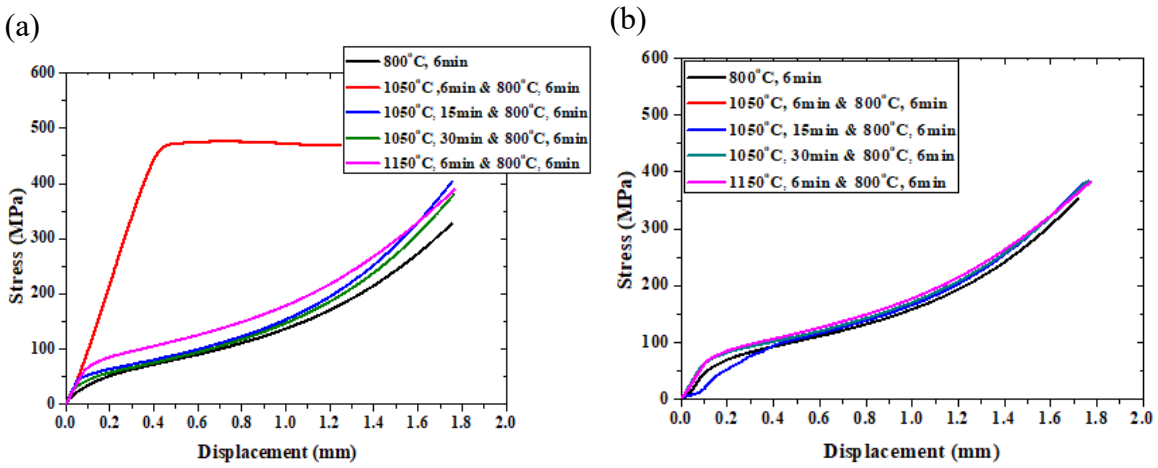

Figure 10 Compression test of ND direction based on Alloy B and Gr.92 with different heat treatment: (a) Alloy B steel and (b) Gr.92 steel.

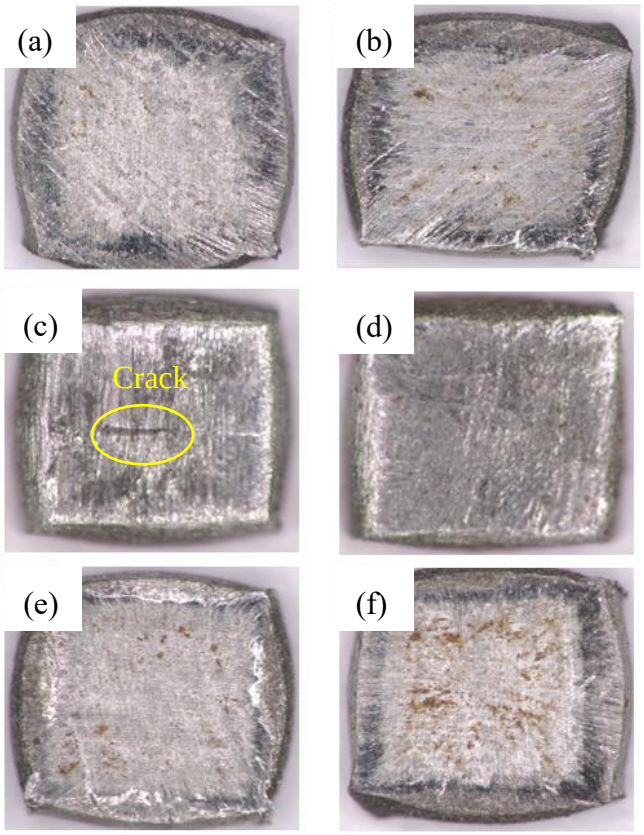

Figure 11 Results of compression test of ND direction based on Alloy B and Gr.92 with different heat treatment: (a) Alloy B 800 °C, 6 minutes (b) Gr.92 800 °C, 6 minutes (c) Alloy B 1050 °C, 6 minutes, and 800 °C, 6 minutes (d) Gr.92 1050 °C, 6 minutes, and 800 °C, 6 minutes (e) Alloy B 1150 °C, 6 minutes, and 800 °C, 6 minutes (e) Gr.92 1150 °C, 6 minutes, and 800 °C, 6 minutes.

4. **Discussion**

This study was investigated the causes of fractures on the microstructural and mechanical properties of Alloy B steel during the manufacturing process. As shown in Figures 3 and 4, the cleavage fracture was only observed Alloy B steel under 1050 °C, 6 minutes, and 800 °C, 6 minutes.

Morpholoiges after the different heat treatment conditions are classified into tempered lath martensite structure and deformed structure. Since the morphologies of tempering heat treatment conditions that the austenite phase transformation did not occur, the deformed structure was remained [20]. On the other hand, the deformed microstructure was transformed into an austenitic structure by heating at the Ar_3 (the temperature at which the α to γ transformation commences on heating) transformation point or higher in the normalized condition[21]. The deformed structure disappears during austenitization, and lath martensite forms with a high dislocation density in the PAG (prior austenite grain boundary) on cooling [22]. The PAGs are divided into packet boundaries parallel to a group of laths with the same habit plane, and each packet boundary is further subdivided into block boundaries with the same orientation as the lath group. The lath and packet are parallel to the {111} plane of the austenite and have K-S orientation relationship [23]. In a packet, there are six variants with different direction parallel relationships on the same conjugate parallel close-packed plane (e.g., $(111)\gamma$ //$(011)\alpha$) [23,24].

However, in the case of Alloy B steel at 1050 °C, 6 minutes, and 800 °C, 6 minutes and remained the deformed structure. The phase transformation temperature (Ar_3) was measured by thermomechanical analysis (TMA) of Alloy B steel and compared with that of 9Cr-1Mo steel [25,26]. As a result, the phase transformation temperatures have higher in the Alloy B steels are shown in the Table 2. This phenomenon may be related to the segregation of boron at grain boundaries. It is well known that segregation affects phase transformation and the recrystallization temperature due to grain boundary energy reduction and other factors [27]. In addition, segregation elements influence the annealing textures following grain boundary segregation. In particular, boron is known to inhibit austenite transformation [28]. It also influences the textures of the two steels because of their different boron contents. It is believed that the texture changes based on the fraction of austenite phase during intercritical annealing of the two steel types. The texture with a strong {111} component develops by intercritical annealing with a certain amount of γ phase transformed during the $\alpha \rightarrow \gamma \rightarrow \alpha$ transformation [29–31]. Therefore, the Alloy B steels with a high phase-transformation temperature did not develop γ-fibers which are components that become parallel to the ND direction as a result of incomplete normalization during the $\alpha \rightarrow \gamma \rightarrow \alpha$ transformation.

Table 2 Phase transformation temperature for Alloy B steel and 9Cr-1Mo steel [25].

	Ac_1	**Ac_3**
9Cr-1Mo	**830**	**875**
Alloy B	**852**	**909**

Figure 10 shows result of the compression test in the ND direction of Alloy B. Specifically, the fracture occurs at the point where hardening rapidly occurs in the elastic region and strength suddenly increases and changes from the elastic region to fracture region. The phenomenon is because the γ-fiber component did not develop on the ND plane and plastic deformation did not occur in the ND plane.

Crack initiation occurs along slip bands in a grain or at grain boundary on the surface. Studies of ferrite steels in crystallographic mode indicated that cleavage involves separation of atomic bonds along the low index {001} crystal plane [32]. The separation process along the low index plane prefers to lower their surface energy. The low index plane is observed to lie on {001} and other low index planes such as {110}, {112}, and {123}. Other studies reported that cleavage fractures are caused by a lack of slip band [33]. Conversely, the Alloy B, 1050 °C, 6 minutes, and 800 °C, 6 minutes condition, appears to cause the aforementioned phenomenon because the slip system does not function properly during rolling This is because the ND // {111} plane (γ-fiber), which ensures that formability does not develop. Thus, it is considered that plastic deformation does not occur on the ND plane and fracture occurs.

5. Conclusion

In the study, the modified 9Cr-2W steel (Alloy B) was developed to improve the creep performance of sodium cooled fast reactor fuel cladding. It is expected that the investigation of the material properties and manufacturing technology of these alloys will significantly contribute to expanding the applicability of components requiring high temperature strength and creep characteristics for nuclear reactors in the future.

The results of the analysis of the fracture occurring during the manufacturing process of Alloy B steel indicated that the increase in the boron content increased the $\alpha \rightarrow \gamma$ phase transformation temperature such that sufficient transformation did not occur in the normalizing condition. We found that the effect of heat treatment depended on the B content. Given the incomplete heat treatment conditions, the γ-fiber components that are advantageous for formability did not develop. Given the aforementioned reasons, it is assumed that cracks occurred at the time of the transition from elastic deformation to plastic deformation in the ND direction during the rolling process, thereby resulting in failure. Therefore, it is necessary to avoid the intermediate heat treatment condition in which γ-fiber does not fully develop, i.e., an imperfect normalization.

Acknowledgments: This work was supported by the National Nuclear R&D program through the Sodium-cooled Fast Reactor Development Agency funded by the Ministry of Science and ICT of South Korea (2012M2A8A2025646).

Author Contributions: All authors were involved in discussing the results and in finalizing the manuscript.

Conflicts of Interest: The authors declare no conflict of interest.

References

1. Kim, J.H.; Baek, J.H.; Kim, S.H.; Lee, C.B.; Na, K.S.; Kim, S.J. Effect of hot rolling process on the mechanical and microstructural property of the 9Cr-1Mo steel. *Ann. Nucl. Energy* **2011**, *38*, 2397–2403.

2. Heo, H.M. Effect of Boron on the Formability of Modified 9Cr-2W steel, Hanyang University, 2019.
3. Jeong, E.H.; Park, S.G.; Kim, S.H.; Kim, Y. Do Evaluation of the effect of B and N on the microstructure of 9Cr–2W steel during an aging treatment for SFR fuel cladding tubes. *J. Nucl. Mater.* **2015**, *467*, 527–533.
4. Heo, H.M.; Jeong, E.H.; Kim, S.H.; Kim, J.R. Comparison between effect of B and N on the microstructure of modi fi ed 9Cr-2W steel during aging and creep. *Mater. Sci. Eng. A* **2016**, *670*, 106–111.
5. Kim, J.H.; Heo, H.M.; Kim, S.H. Effect of an intermediate process on the microstructure and mechanical properties of HT9 fuel gadding. *J. Korean Inst. Met. Mater.* **2013**, *51*, 893–900.
6. György, H.; Czifrus, S. Investigation on the potential use of thorium as fuel for the Sodium-cooled Fast Reactor. *Ann. Nucl. Energy* **2017**, *103*, 238–250.
7. Kim, J.T.; Jae, M.S. A study on reliability assessment of a decay heat removal system for a sodium-cooled fast reactor. *Ann. Nucl. Energy* **2018**, *120*, 534–539.
8. Kim, T.K.; Kim, S.H.; Lee, C.B. Effects of an intermediate heat treatment during a cold rolling on the tensile strength of a 9Cr-2W steel. *Ann. Nucl. Energy* **2009**, *36*, 1103–1107.
9. Garner, F.A.; Toloczko, M.B.; Sencer, B.H. Comparison of swelling and irradiation creep behavior of fcc-austenitic and bcc-ferritic/martensitic alloys at high neutron exposure. *J. Nucl. Mater.* **2000**, *276*, 123–142.
10. Lee, C.B.; Cheon, J.S.; Kim, S.H.; Park, J.Y.; Joo, H.K. Metal Fuel Development and Verification for Prototype Generation IV Sodium-Cooled Fast Reactor. *Nucl. Eng. Technol.* **2016**, *48*, 1096–1108.
11. Kim, S.H.; Song, B.J.; Ryu, W.S.; Hong, J.H. Creep rupture properties of nitrogen added 10Cr ferritic/martensitic steels. *J. Nucl. Mater.* **2004**, *329–333*, 299–303.
12. Jeong, E.H.; Kim, J.H.; Kim, S.H.; Kim, Y. Do Influence of B and N on the microstructural characteristics and high-temperature strength of 9Cr-2W steel during an aging treatment. *Mater. Sci. Eng. A* **2017**, *700*, 701–706.
13. Bunge, H.J. *Texture Analysis in Materials Science*; Butterworths: London, 1982; ISBN 9780408106429.
14. Choi, S.H.; Jin, Y.S. Evaluation of stored energy in cold-rolled steels from EBSD data. *Mater. Sci. Eng. A* **2004**, *371*, 149–159.
15. Abe, H.; Furugen, M. Evaluation Method of Workability in Cold Pilgering of Zirconium-based Alloy Tube. *Mater. Trans.* **2010**, *51*, 1200–1205.
16. Abe, H.; Furugen, M. Method of evaluating workability in cold pilgering. *J. Mater. Process. Technol.* **2012**, *212*, 1687–1693.
17. Heo, H.-M.; Kim, J.-H.; Kim, S.-H.; Kim, J.-R. Evaluation of workability on the microstructure and mechanical property of modified 9Cr-2W steel for fuel cladding by cold drawing process and intermediate heat treatment condition. *Metals (Basel).* **2018**, *8*, 1–13.
18. Humphreys, F.J.; Hatherly, M. *Recrystallization and Related Annealing Phenomena*; Sleeman, D., Ed.; Elsevier, 2012; ISBN 9788578110796.
19. Huh, M.Y.; Engler, O. Effect of intermediate annealing on texture, formability and ridging of 17%Cr ferritic stainless steel sheet. *Mater. Sci. Eng. A* **2001**, *308*, 74–87.

20. Birosca, S.; Ding, R.; Ooi, S.; Buckingham, R.; Coleman, C.; Dicks, K. Nanostructure characterisation of flow-formed Cr–Mo–V steel using transmission Kikuchi diffraction technique. *Ultramicroscopy* **2015**, *153*, 1–8.
21. Klueh, R.L.; Harries, D.R. *High-Chromium Ferritic and Martensitic Steels for Nuclear Applications*; ASTM International, 2001; ISBN 978-0-8031-2090-7.
22. Saroja, S.; Vijayalakshmi, M.; V.S., R. Influence of cooling rates on the transformation behaviour of 9Cr-1 Mo-O.07C steel. *J. Mater. Sci.* **1992**, *27*, 2389–2396.
23. Morito, S.; Huang, X.; Furuhara, T.; Maki, T.; Hansen, N. The morphology and crystallography of lath martensite in Fe-C alloy steels. *Acta Mater.* **2006**, *54*, 5323–5331.
24. Maki, T. Morphology and substructure of martensite in steels. *Phase Transform. Steels* **2012**, *2*, 34–58.
25. Raju, S.; Ganesh, B.J.; Banerjee, A.; Mohandas, E. Characterisation of thermal stability and phase transformation energetics in tempered 9Cr-1Mo steel using drop and differential scanning calorimetry. *Mater. Sci. Eng. A* **2007**, *465*, 29–37.
26. Shrestha, T.; Alsagabi, S.; Charit, I.; Potirniche, G.; Glazoff, M. Effect of Heat Treatment on Microstructure and Hardness of Grade 91 Steel. *Metals (Basel).* **2015**, *5*, 131–149.
27. Briant, C.L. *Impurities in Engineering Materials: Impact, Reliability and Control*; Dekker, M., Ed.; Routledge: New York and Basel, 1999;
28. El-Shennawy, M.; Farahat, A.I.; Masoud, M.I.; Abdel-Aziz, A.I. Effect of Boron Content on Metallurgical and Mechanical. *Int. J. Mech. Eng.* **2016**, *5*, 1–14.
29. Vivas, J.; Capdevila, C.; Jimenez, J.; Benito-Alfonso, M.; San-Martin, D. Effect of Ausforming Temperature on the Microstructure of G91 Steel. *Metals (Basel).* **2017**, *7*, 236.
30. HASHIMOTO, O.; SATOH, S.; TANAKA, T. Development of {111} Texture in Intercritical Annealing of Low Carbon Steels. **1987**, *27*, 746–754.
31. Obasi, G.C.; Birosca, S.; Quinta Da Fonseca, J.; Preuss, M. Effect of β grain growth on variant selection and texture memory effect during $\alpha \rightarrow \beta \rightarrow \alpha$ phase transformation in Ti-6 Al-4 v. Acta Mater. 2012, 60, 1048–1058.
32. Tu, M.Y.; Hsu, C.A.; Wang, W.H.; Hsu, Y.F. Comparison of microstructure and mechanical behavior of lower bainite and tempered martensite in JIS SK5 steel. *Mater. Chem. Phys.* **2008**, *107*, 418–425.
33. Gross, D.; Thomas Seelig *Fracture Mechanics With an Introduction to Micromechanics*; Ling, F.F., Ed.; 2011; ISBN 9781118147757.